Analysis of Results from Large-Scale Wave-Current Laboratory Experiments

Jessica R. Lacy
U.S. Geological Survey
Coastal and Marine Geology Program
400 Natural Bridges Drive
Santa Cruz, CA 95060
Phone: 831-427-4720; fax: 831-427-4748; Email: jlacy@usgs.gov

David M. Rubin
Phone: 831-427-4736; Email: drubin@usgs.gov

Document Number N00014-09IP20007

LONG-TERM GOALS

To explain the evolution, dynamics, and morphology of bedforms found in sandy inner-shelf environments, using laboratory and field observations and numerical modeling.

OBJECTIVES

Our objective is to analyze existing laboratory data including measured suspended sediment profiles and ripple wavelengths during ripple evolution, and observations of bedform migration, and to use the results to support calibration of a Large Eddy Simulation of ripple evolution under development by Fringer and Chou at Stanford University. Specifically, we aim to

- Analyze the relationship between time-averaged suspended sediment profiles and bedform dimensions, wave energy, and current speed.
- Compare results to existing analytical models, and develop new parameterization of these relationships if merited.
- Analyze bedform migration and bedload transport from flume experiment sonar data, and relate to flow conditions.
- Provide data sets and analytical results to Fringer and Chou for model testing.

APPROACH

We are working with data we collected in experiments that studied ripples formed under combined waves and currents in the large flume in Tsukuba, Japan as part of the Ripples DRI. Several aspects of the data set make it suitable for model calibration. It documents ripple evolution under non-collinear waves and currents in a laboratory setting, where initial bed conditions and the history of forcing is known. In addition the wave velocities, wave periods, and grain size in the experiments are the same scale as in coastal environments. We know of only two other laboratory studies of ripples produced by non-collinear waves and currents: Khelifa and Ouellet 2000 and Andersen and Faraci 2003. In both of these investigations maximum ratios of wave orbital diameter to median grain size d_o/D were less than 650, while our maximum d_o/D was greater than 3500. In addition, our data set includes time series of

Report Documentation Page

Form Approved
OMB No. 0704-0188

1. REPORT DATE **2009**	2. REPORT TYPE	3. DATES COVERED **00-00-2009 to 00-00-2009**

4. TITLE AND SUBTITLE **Analysis of Results from Large-Scale Wave-Current Laboratory Experiments**	5a. CONTRACT NUMBER
	5b. GRANT NUMBER
	5c. PROGRAM ELEMENT NUMBER
6. AUTHOR(S)	5d. PROJECT NUMBER
	5e. TASK NUMBER
	5f. WORK UNIT NUMBER
7. PERFORMING ORGANIZATION NAME(S) AND ADDRESS(ES) **U.S. Geological Survey,Coastal and Marine Geology Program,400 Natural Bridges Drive,Santa Cruz,CA,95060**	8. PERFORMING ORGANIZATION REPORT NUMBER
9. SPONSORING/MONITORING AGENCY NAME(S) AND ADDRESS(ES)	10. SPONSOR/MONITOR’S ACRONYM(S)
	11. SPONSOR/MONITOR’S REPORT NUMBER(S)

12. DISTRIBUTION/AVAILABILITY STATEMENT
Approved for public release; distribution unlimited

13. SUPPLEMENTARY NOTES

14. ABSTRACT

15. SUBJECT TERMS

16. SECURITY CLASSIFICATION OF:			17. LIMITATION OF ABSTRACT	18. NUMBER OF PAGES	19a. NAME OF RESPONSIBLE PERSON
a. REPORT **unclassified**	b. ABSTRACT **unclassified**	c. THIS PAGE **unclassified**	**Same as Report (SAR)**	**10**	

Standard Form 298 (Rev. 8-98)
Prescribed by ANSI Std Z39-18

wavelength, extracted from sonar data, and of profiles of suspended sediment, from the initial flat bed to final equilibrium bed state. There are a number of laboratory studies of ripples produced by waves alone that provide data on suspended-sediment concentrations (SSC) closer to the bed than ours (e.g van der Werf et al., 2006), or on ripple evolution (e.g. Faraci and Foti, 2002; Smith and Sleath, 2005) that could provide additional data for model calibration.

Both bedload and suspended-sediment transport contribute to ripple evolution, migration, and scouring. The relative importance of the two processes depends on flow conditions. Although physically bedload and suspended-sediment transport represent a continuum of response to bed shear stress, in most hydrodynamics models of bedform evolution (including that of Fringer and Chou) the two processes are represented by separate (linked) components of the model. The suspended-sediment data from the flume experiments will be used to calibrate SSC in the model, which is critical to predictions of suspended-sediment transport as well as ripple evolution.

WORK COMPLETED

Our analysis of the bedforms and hydrodynamic conditions in the 2005 flume experiments was published in the Journal of Geophysical Research (Lacy et al. 2007). Lacy presented results of the bedform analysis at the Fall AGU meeting in December 2006. She presented analysis of suspended-sediment concentration (SSC) profiles from the experiments at the 2008 International Conference on Coastal Engineering in Hamburg, Germany, and at the 2008 Fall AGU meeting. We have processed and provided data to Fringer and Chou for comparison with results from their bedform evolution model, as well as collaborating on approaches for modeling bedload transport, strategies for comparing model output to data, and identifying potential model improvements. Lacy served on the Reading Committee for Chou's PhD dissertation, and co-authored a poster with Chou at the 2009 Fall AGU meeting.

RESULTS

The laboratory experiments used an oscillating plate system in a unidirectional flume to produce non-collinear currents and oscillating flows (to simulate near-bed wave velocities). The four-meter width of the flume allowed us to create combined wave-current flows on the same scale as those that produce bedforms in the natural environment. Results relating bedforms to experimental wave and current conditions were described in previous progress reports and in Lacy et al. 2007, and are summarized here.

There were twenty runs of approximately 40 minute duration with varying wave-current conditions. Current velocities ranged from 0 to 26 cm/s, maximum oscillatory velocities ranged from 16 to 40 cm/s, oscillation period was 8 or 12 s, and the angle between waves and currents was 45°, 60°, or 90°. Median sediment grain diameter was 0.27 mm. An instrumented frame mounted on the oscillating tray held two acoustic Doppler velocimeters (ADV) to measure tray motions and current velocities at 5 cm and 13 cm above the bed, two imaging sonars to monitor bedform evolution, and an Acoustic Backscatter Sensor (ABS) to measure profiles of suspended sediment concentration (Figure 1). After each run the bed test-section was photographed and bedform height and wavelength were measured manually. The bedforms varied from linear ripples to strongly three-dimensional structures.

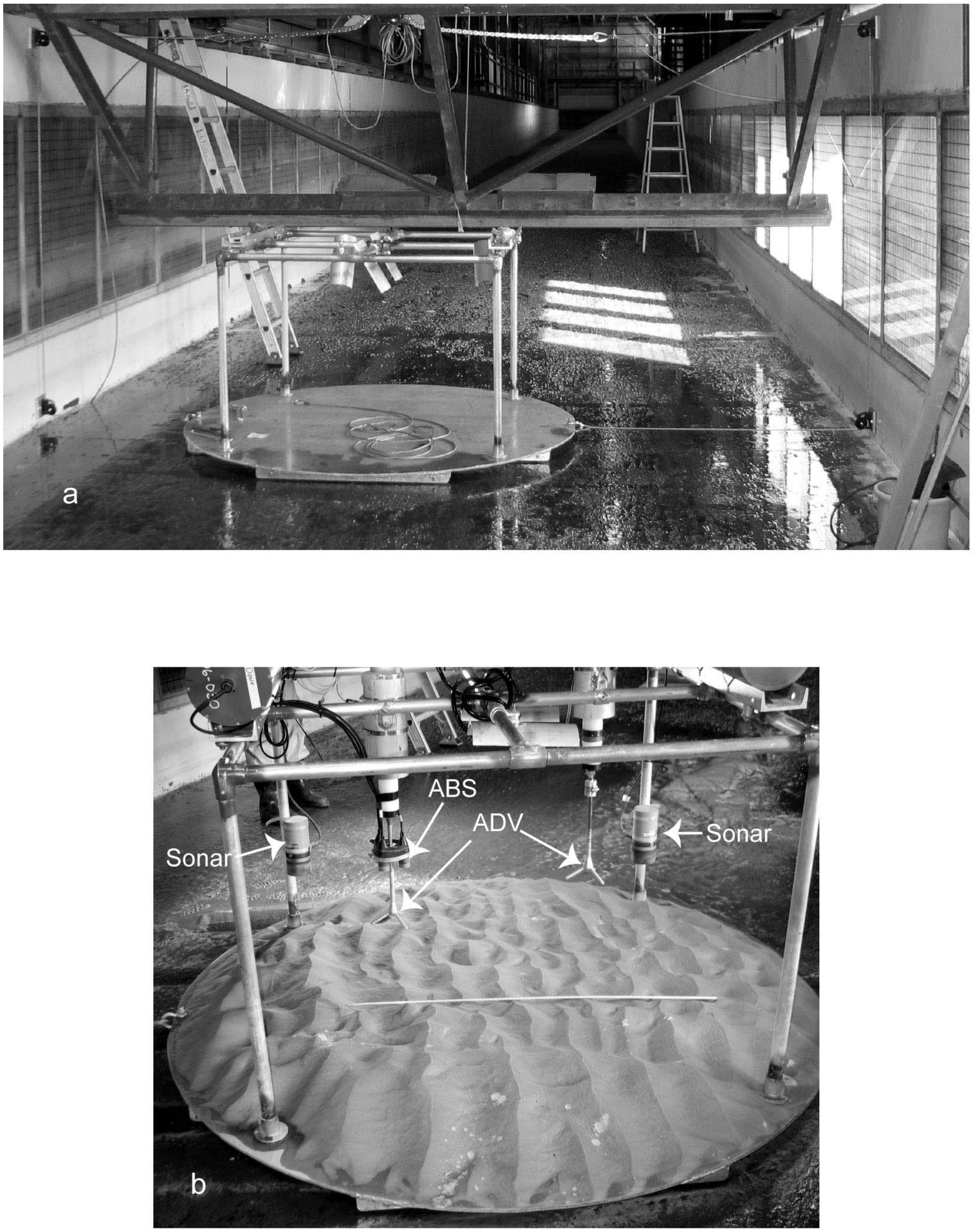

Figure 1: Photographs of experimental setup: a) flume with oscillating plate, b) oscillating plate showing position of instrumentation, at the end of a run with oscillation excursion of 60 cm and current of 14 cm/s.

Experimental runs typically started from a flat bed, and bedforms developed to near-steady state, as documented in sonar images (Figure 2). Ripple wavelength and crest orientations during the runs were extracted from sonar images using 2D Fourier decomposition (FFT). The difference between

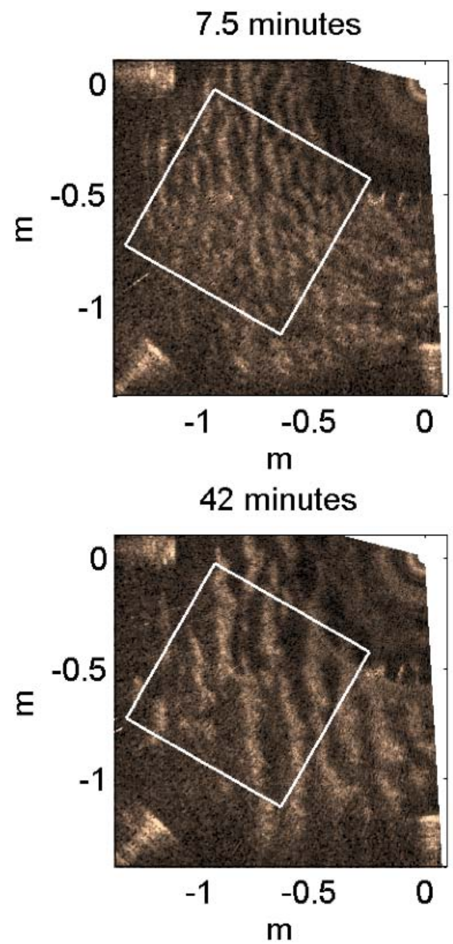

Figure 2: The growth of ripples between 7.5 and 42 minutes in the experiment during run 9 (wave velocity24 cm/s, current speed of 6 cm/s, and final ripple height 2.0 cm). White boxes indicate the portion of the bed used to determine ripple wavelength and orientation using two dimensional Fourier decomposition.

initial and final ripple wave number decreased exponentially as a function of wave period. The typical time for evolution to 90% of the final wave number was approximately 160 wave periods. Evolution time decreased with increasing current speed. Use of a combined wave-current orbital excursion improved agreement of the response of ripple wavelength to wave energy in the experiments with published predictors of wave ripples. In general, wavelength decreased with increasing current strength. Three-dimensionality, based on the circular variance of the crest orientations from the FFTs, increased with wave orbital diameter d_o and with the ratio of current to wave energy.

The distribution of crest orientations was determined from averaged FFT results from the two sonars to minimize bias due to beam direction. Maximum gross bedform-normal transport (Rubin and Hunter, 1987) and wave directions are equally good predictors of crest orientation for this data, and are much better predictors than the directions of current or maximum wave-current bed shear stress.

The next phase of work involved the suspended-sediment data. System constants for the ABS were determined from laboratory backscatter data, and used to calibrate the backscatter data to concentration.

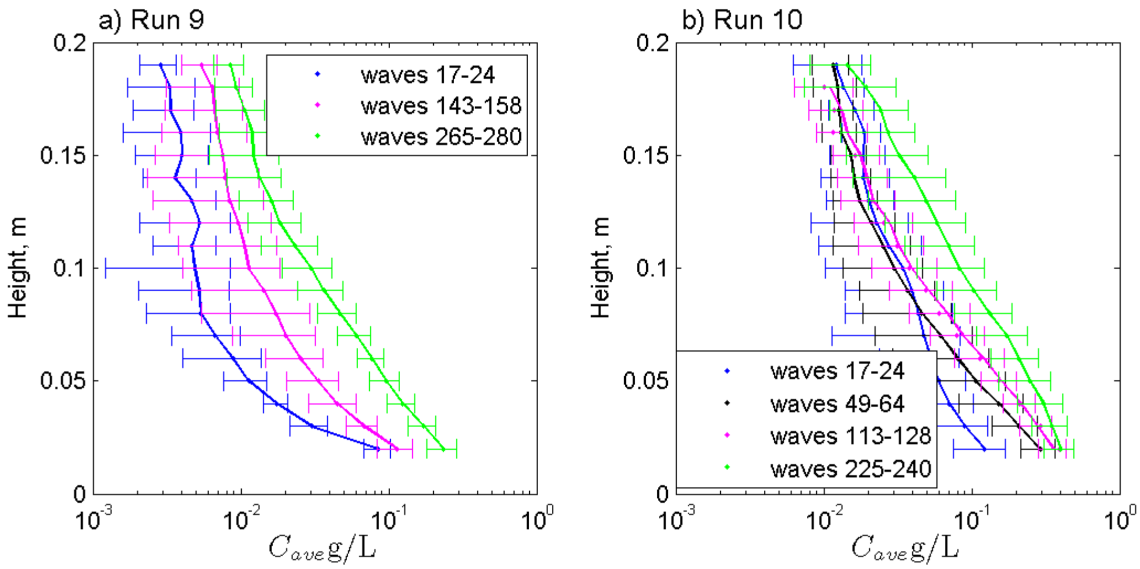

Figure 3: Averaged suspended-sediment concentration (SSC) measured by the ABS at beginning, middle, and end of run 9 (wave velocity 29 cm/s, current speed 7 cm/s, and final ripple height 2 cm), and at beginning, end and two intermediate points during run 10 (wave velocity 39 cm/s, current speed of 6 cm/s, and final ripple height 4.6 cm). In both runs wave-current angle was 90º and bed was initially flat. Error bars show standard deviation of 8 second (one wave period) averages.

The vertical position of the data was corrected to height above the bed (as detected by the ABS) rather than distance from the transducer, to account for changes in bed elevation during the runs. Returns less than 2 cm from the bed were discarded due to the potential for spreading of strong backscatter off the bed into adjacent cells (vertical resolution of SSC profiles is 1 cm). Concentrations were calculated from the data from the highest frequency of the three ABS transducers (5 MHz), because the backscatter was within the calibration range for the greatest number of runs for this frequency. Instantaneous concentrations were highly variable, and we found that determination of a quasi-steady-state concentration $\overline{C}$ requires averaging 1-2 minutes of the 8 Hz data. Note that this averaging period could overlap the timescale of migration of bedform troughs or crests past the sensor. $\overline{C}$ typically increased significantly as bedforms evolved (Figure 2), as expected. Final concentrations and $\overline{C}$ profile shape varied with the final bedform height, wave energy, and current speed.

We identified an important limitation to the suspended sediment data, caused by the experimental set-up. The absence of sand on the flume floor, outside of the oscillating plate, limited the time available for vertical mixing of sediment to the travel time over the plate. For large oscillations, the ABS moved laterally into a region that is not continuously over the plate once per oscillation, reducing sediment supply for these runs. In addition, the current introduces clear water at the upstream edge of the plate. The ABS measured concentration profiles 108 cm from the upstream edge of the plate. Travel times to this position on the plate range from approximately two wave periods for 7 cm/s currents, to less than half a wave period for 30 cm/s currents, for 8 second waves. The height above the bed influenced by turbulent mixing of bed sediment decreases with the reduced travel times at the higher current speeds. Thus observed differences in profiles for different current speeds may be caused, in part, by differences in this effective mixing length scale.

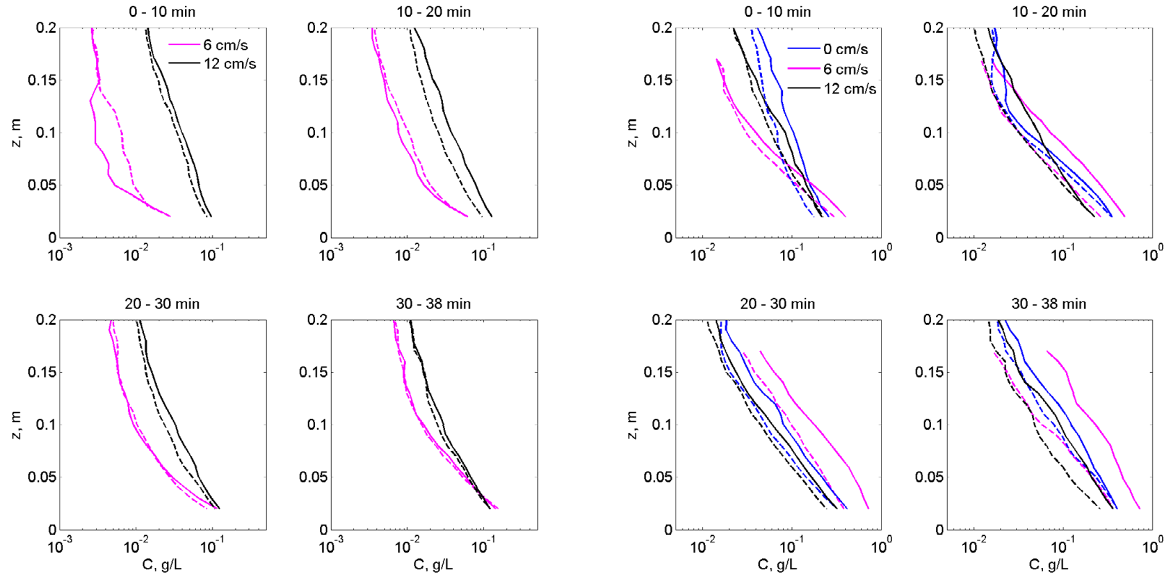

Figure 4: Average suspended-sediment concentration profiles for half-oscillation with continuous sediment supply (solid lines) and semi-oscillation with reduced sediment supply (dashed lines), for four intervals in each run. Subplots on left for smaller oscillations (A = 0.3 m), subplots on right for larger oscillations (A = 0.4m). Color indicates current speed (see legends). Angle between current and oscillations is 90 degrees.

To determine the effect of sediment limitation during large oscillations on SSC profiles, phase-averaged profiles from the semi-oscillations that are not supply limited (+x direction) were compared to the semi-oscillation with reduced sediment supply (-x direction). (Figure 4). For 60-cm oscillations (A = 0.3), there is no detectable difference between the two phases. For higher amplitude oscillations the semi-oscillation in the +x direction produces SS concentration up to 2.5 times greater than for the -x semi-oscillation. The difference increases over the course of the run, and is greater for runs with larger bed forms. We conclude that the profiles from the 60-cm oscillation runs are suitable for model calibration, and that for the larger amplitude oscillation runs, averages of the semi-oscillations that are not supply limited should be used.

The influence of the clear water advected by the current is more difficult to test. As the water travels downstream over the plate, near-bed suspended sediment is turbulently mixed upwards into the clear water. Scaling suggests that bed sediment is turbulently mixed over the bottom 15 cm of the profile for u = 6 cm/s, and over the bottom 10 cm for u = 12 cm/s, during travel over the 1-m distance across the plate to the ABS. This indicates that this lower portion of the profiles can be used for model comparisons (using averages from the semi-oscillations in the +x direction).

Bedform evolution and migration are not significantly influenced by the inconsistent sediment supply, because they are governed by bedload and near-bed suspended sediment transport. At the edges of the plate bedforms were influenced by edge effects, but in the central region of the 2-m diameter plate bedform dimensions were uniform.

Combined data sets document evolution of ripple dimensions, $\overline{C}$, and turbulence (Figure 5). In Figure 3, reference concentration was estimated by extrapolating a semilog least-squares fit of 128-second

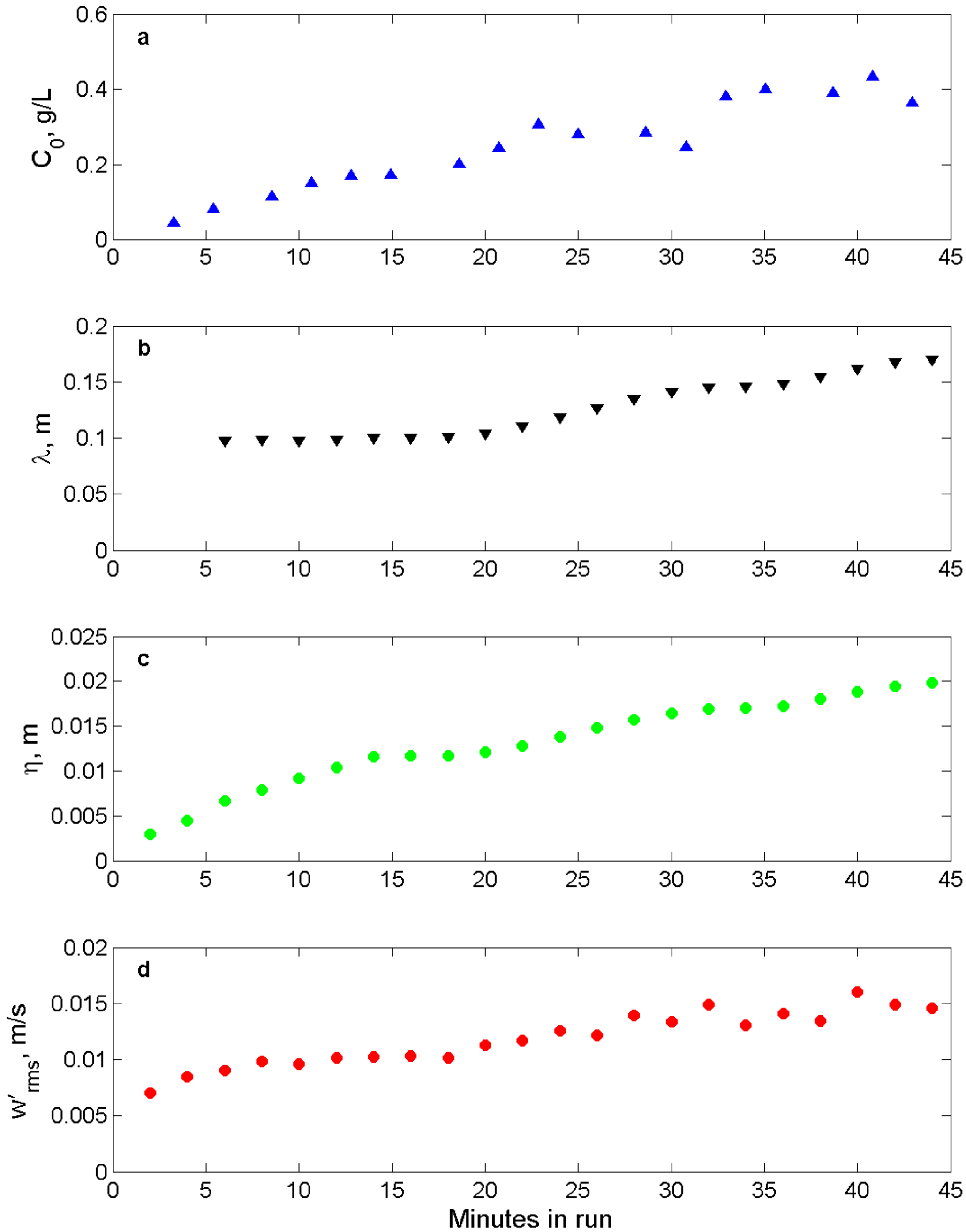

Figure 5: Time series of a) reference concentration, b) ripple wavelength, c) ripple height, and d) root-mean-square vertical velocity for a run with current speed of 7 cm/s and wave orbital velocity of 31 cm/s (Run 9). Wave-current angle was 90º.

averaged $\overline{C}$ from the bottom 3 cells of the ABS data to the bed elevation. Ripple wavelength λ was calculated from the sonar images using two-dimensional Fourier analysis (for details see Lacy et al., 2007). Time-varying estimates of η were calculated from the final measured ripple dimensions and the time series of λ, assuming constant slope, except during the first five minutes of each run. During this initial period the evolution of ripple height (from flat bed) was assumed to follow an exponential growth model (Smith and Sleath, 2005). The root-mean-square vertical velocities in Figure 3 are an index of turbulence intensity. Reynolds stresses were also calculated. Both turbulence statistics were calculated from two-minute segments of 10-Hz ADV data, high-pass filtered to remove the influence of plate oscillations.

Model-data comparison

Bedform dimensions and orientations derived from the sonar images, as well as the images themselves, were used to inform and calibrate the Chou and Fringer large-eddy simulation model for ripple evolution (Chou and Fringer, submitted).

Comparison of results from the first 5 minutes of the runs is encouraging. The model simulations are

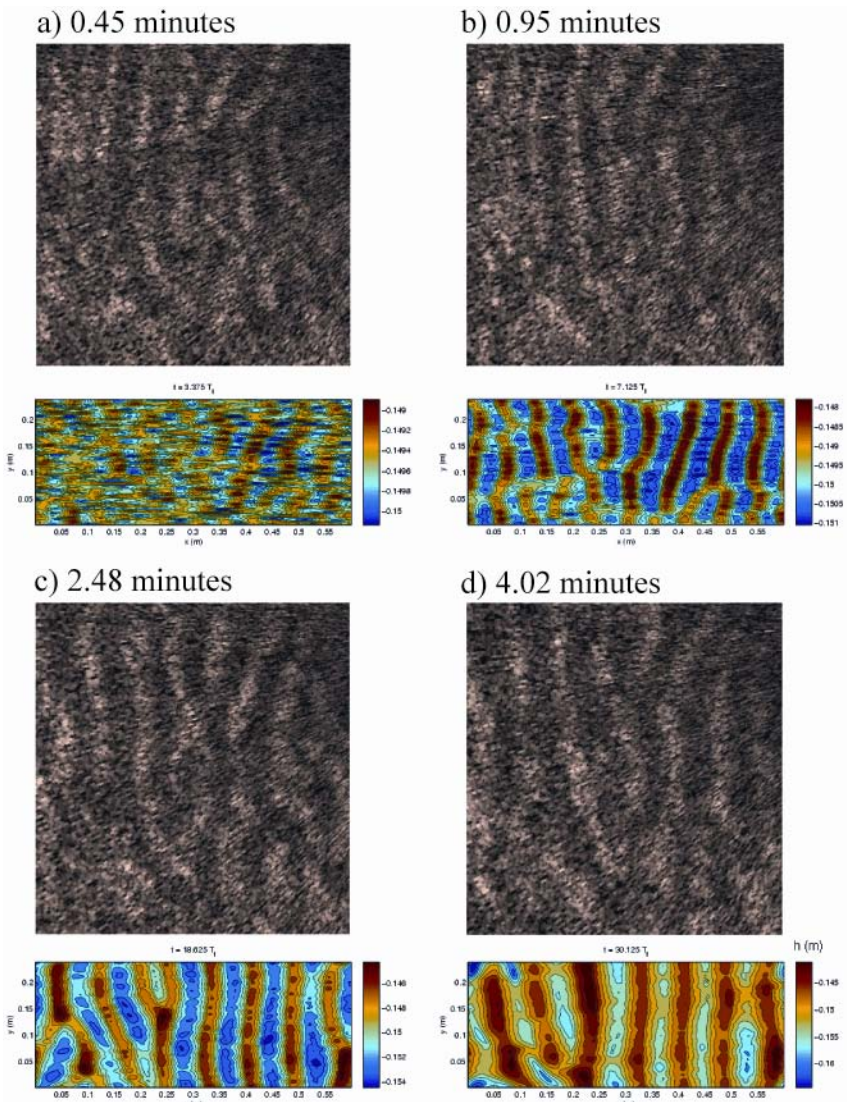

Figure 4: Comparison of bed elevations simulated with Chou and Fringer model (below) to sonar images(above) from experimental run 11 (wave velocity 39 cm/s and no current) at a) 0.45, b) 0.95, c) 2.48 and d) 4.02 minutes after run began. Run duration was 38 minutes.

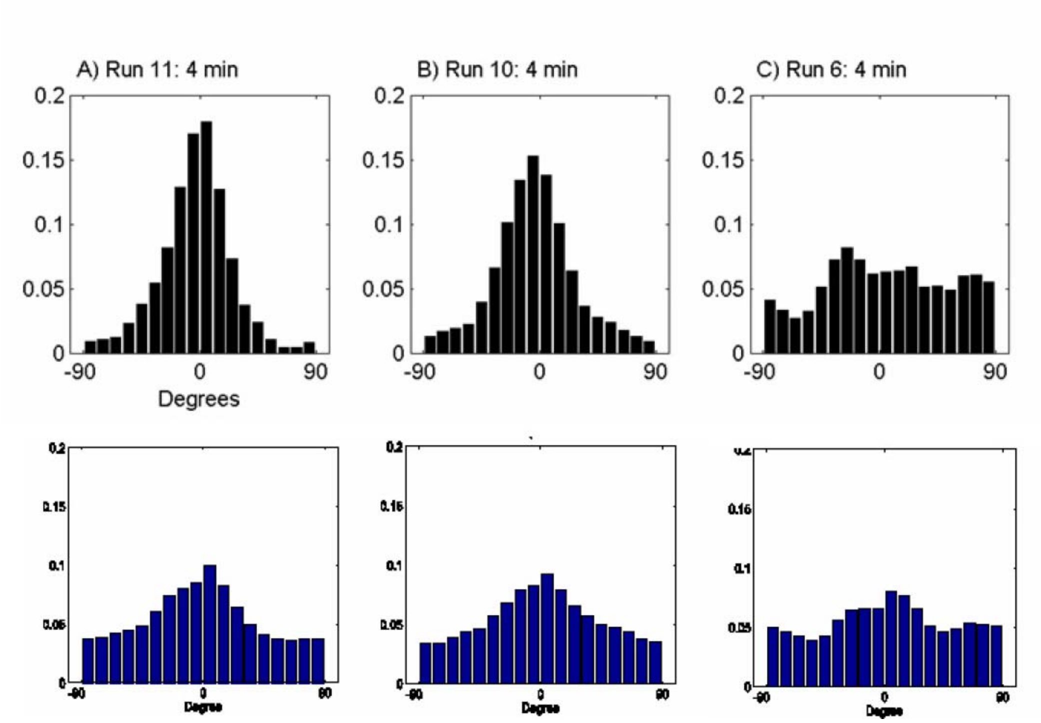

Figure 5: Histograms of bedform orientation from Fourier decomposition of sonar data (above) and simulated bed elevations(below) after 4 minutes in a) run 11 (wave velocity 39 cm/s and no current) at b) Run 10 (wave velocity 39 cm/s and 7 cm/s current) and c) run 6(wave velocity 39 cm/s and 24 cm/s current).

computationally intensive (5 minutes of experiment time requires 21 days of computation time on 40 processors), and runs simulating the full duration of the experimental runs have not yet been completed. The rate of evolution of bedform wavelength in the simulations is quite consistent with the data, as are features such as bedform merging, which is indicative of the process of ripple growth (Figure 4). Comparisons between runs show that three-dimensionality of bedforms, measured by the variance in orientations measured by Fourier decomposition, increases with increasing ratio of current to wave velocities in the simulations, as it does in the data (Figure 5).

IMPACT/APPLICATION

The flume experiments are the first laboratory investigation of ripples formed by non-collinear waves and currents at full scale (i.e. realistic wave periods and wave excursions), and that document ripple evolution. The results provide an important contribution to understanding the types, dimensions, and orientation of ripples produced by combined flows, and to the development of empirical models relating ripple morphology to hydrodynamic conditions and grain size. In addition, the flume experiments provide calibration data for the development of process-based numerical models of ripple evolution, which are needed to advance understanding of the physical processes governing ripple evolution and morphology.

RELATED PROJECTS

Work described in this report involves active collaboration with Oliver Fringer at Stanford University in his development of an LES model of ripple evolution.

Rubin and Lacy deployed a real-time sediment transport and seafloor observatory adjacent to the Santa Cruz, CA wharf in November, 2008 (USGS funded). Instruments measure bed sediment grain size, bedform morphology, wave and current velocities, and suspended sediment grain size on hourly timescales. The data will be used to investigate bedform evolution and the relationship between bed and suspended sediment grain size distributions, and to further test whether bedform orientation is governed by the direction of maximum gross bedform-normal transport. We are also gauging sediment supply from the San Lorenzo River, and examining seasonal cycling of river-derived sediments at the observatory site on the inner shelf.

REFERENCES

Andersen, K.H., and C.Faraci. 2003. The wave plus current flow over vortex ripples at an arbitrary angle. *Coastal Engineering* 47: 431-441.

Chou, Y.J, and O.B. Fringer. A model for the simulation of coupled flow-bedform evolution in turbulent flows. Submitted to *Journal of Geophysical Research*.

Khelifa, A., and Y. Ouellet. 2000. Prediction of sand ripple geometry under waves and currents. *Journal of Waterway, Port, Coastal, and Ocean Engineering* 126 (1): 14-22.

Faraci, C., and E. Foti. 2002. Geometry, migration and evolution of small-scale bedforms generated by regular and irregular waves. *Coastal Engineering* 47: 35-52.

Lacy, J. R., Rubin, D. M., Ikeda, H., Mokudai, K., and D. M. Hanes, 2007. Bedforms created by simulated waves and currents in a large flume. *Journal of Geophysical Research* , 112, C10018, doi:10.1029/2006JC003942.

Rubin, D.M., and R.E. Hunter, 1987. Bedform alignment in directionally-varying flows. *Science*, 237, 276-278.

Smith, D., and J.F.A. Sleath. 2005. Transient ripples in oscillatory flow. *Continental Shelf Research* 25: 485-501.

van der Werf, J.J., J.S. Ribberink, T.O'Donoghue, and J.S. Doucette. 2006. Modelling and measurement of sand transport processes over full-scale ripples in oscillatory flow. *Coastal Engineering* 53: 657-673.

PUBLICATIONS

Lacy, J. R., Rubin, D. M., Ikeda, H., Mokudai, K., and D. M. Hanes, 2007. Bedforms created by simulated waves and currents in a large flume. *Journal of Geophysical Research* , 112, C10018, doi:10.1029/2006JC003942 [Published, refereed].